Solar Energy Materials & Solar Cells 153 (2016) 18–24

Contents lists available at ScienceDirect

Solar Energy Materials & Solar Cells

journal homepage: www.elsevier.com/locate/solmat

Versatile strategies for improving the performance of diamond wire sawn mc-Si solar cells

Y.F. Zhuang [a], S.H. Zhong [a], Z.G. Huang [a,b], W.Z. Shen [a,c,*]

[a] Institute of Solar Energy, and Key Laboratory of Artificial Structures and Quantum Control (Ministry of Education), Department of Physics and Astronomy, Shanghai Jiao Tong University, Shanghai 200240, People's Republic of China
[b] School of Science, Huaihai Institute of Technology, Lianyungang 222005, Jiangsu Province, People's Republic of China
[c] Collaborative Innovation Center of Advanced Microstructures, Nanjing 210093, People's Republic of China

ARTICLE INFO

Article history:
Received 26 November 2015
Received in revised form
6 April 2016
Accepted 7 April 2016

Keywords:
Solar cell
Diamond wire sawn
Multicrystalline silicon
Metal-catalyzed chemical etching
Nano/micro-texture

ABSTRACT

Unlike conventional multi-wire sawn (CMWS) multi-crystalline silicon (mc-Si) wafers, diamond wire sawn (DWS) mc-Si wafers textured by conventional acidic solution of HF/HNO_3 are not suitable for solar cells because visible saw marks set significant barriers in both cell performance and surface appearance. In this work, we have employed versatile strategies based on metal-assisted chemical etching (MACE) technique to eliminate the saw marks and realize effective surface textures on DWS mc-Si wafers, including nano-texture (N-T), micro-texture (M-T) and nano/micro-texture (N/M-T). Especially, benefiting from the tradeoff between optical gain and electrical loss, the efficiency of 18.45% for N/M-T based DWS mc-Si solar cells with a standard wafer size of $156 \times 156\ mm^2$ is reported to be higher by an absolute 0.57% compared with that of CMWS mc-Si solar cells (17.88%). Our work provides ways of fabricating DWS mc-Si solar cells with high efficiencies and satisfactory visual appearance.

1. Introduction

Diamond wire sawing (DWS) technique is widely used in cutting hard and brittle non-metallic materials [1]. In the photovoltaic (PV) industry, DWS has been used in slicing single crystalline silicon (sc-Si) and multi-crystalline silicon (mc-Si) in recent years. Compared with conventional multi-wire sawing (CMWS) with slurry of SiC abrasives, DWS has several advantages including higher productivity, lower material waste, higher precision in cutting thin wafers and less surface mechanical damages [2–6]. More importantly, the conversion efficiency (η) of DWS sc-Si solar cells is over 19% in a traditional industrial production line [7], which is comparable to the η of slurry sawn ones. Therefore, DWS is expected to become the mainstream technique for Si-based solar cells in the near future.

Unfortunately, the production of DWS mc-Si solar cells is not so successful due to the ineffective surface texturization. In the PV industry, acidic solution of HF/HNO_3 is most commonly used in fabricating CMWS mc-Si solar cells [8,9]. During the etching, the surface defects are removed and micron-pits are formed randomly. Unlike CMWS wafers, which are characterized by a thicker damaged layer with random distribution of broken crystals, a lower rough surface with parallel deep saw marks is observed on DWS wafers [2,10]. Resulting from nonuniform etching of the saw marks, DWS mc-Si wafers cannot form an effective texture by this method and the surface reflectance is still higher than 25% [8,11]. Since 80% of mc-Si wafers will be sawn with diamond wires by 2020 [12], it is an urgent affair to realize an effective texture method for DWS mc-Si wafers.

Although reactive ion etching is effective for texturization of mc-Si wafers [13,14], it is not suitable for the PV industry due to the high cost. On the other hand, recent researches shows that effective surface textures with Si nanostructures can be easily formed on silicon wafers by metal-assisted chemical etching (MACE) [15–18], which is simple, cost-effective and compatible with current production lines. In this study, we present versatile strategies to realize effective surface textures on DWS mc-Si wafers based on the MACE technique, including nano-texture (N-T), micro-texture (M-T) and nano/micro-texture (N/M-T). We have demonstrated that all the N-T, M-T and N/M-T based solar cells exhibit higher η than the conventional micro-textured (CM-T) cells. Especially, for the N/M-T based cells, their average η is increased by 0.57% absolutely, reaching 18.45% on a large wafer size of $156 \times 156\ mm^2$, which is attributed to its both better optical and electrical properties. Furthermore, our results reveal that the saw marks have negative influence on the electrical properties of the solar cells but fortunately can be resolved by our texturing methods.

* Corresponding author.
E-mail address: wzshen@sjtu.edu.cn (W.Z. Shen).

http://dx.doi.org/10.1016/j.solmat.2016.04.014
0927-0248/

2. Experimental

2.1. Texturization of diamond wire sawn wafers

In this work, the used silicon wafers were p-type DWS mc-Si with a size of 156×156 mm^2, a thickness of 200 ± 20 μm and resistivity of 1–3 Ω cm. The main steps for texturization of the wafers are shown in Fig. 1. Deionized water (DIW) cleaning was performed after every step. CM-T was prepared by immersing the wafers in the mixed acid solution of HF:HNO_3:DIW = 1:5:4 (volume ratio) for 3 min at 8 °C. N-T, M-T and N/M-T were obtained by multiple-etching processes based on MACE technique. The wafers were firstly dipped into MACE solution (2.6 M HF/1.1 M H_2O_2/0.0002 M $AgNO_3$) for 5 mins at 45 °C. In this process, Ag nanoparticles were deposited onto the silicon and nano-holes were obtained. After that, one group of the wafers were placed in the etching solution of NaOH (5 wt%) for 5 min to form the N-T. Another group of the wafers were immersed into the HF/HNO_3 mixed solution for 3 min at 8 °C. As a result, nano-holes were expanded, and M-T was obtained. Then, a set of the M-T wafers were placed in MACE solution for 5 min again, followed by NaOH etching for 5 min to form the N/M-T. Finally, all the textured wafers were immersed in the HNO_3:DIW = 1:1 (volume ration) for 10 min to remove the residual metal impurities, followed by rinsing with DIW and spin-drying. Here, after all the processes, the removing of the silicon wafers is about 3–4 μm on each side.

2.2. Fabrication of the DWS mc-Si solar cells

After the texturization, all the wafers underwent the same standard industrial solar cell fabricating process, including diffusion, SiN_x:H coating and screen printing. The wafers were firstly placed in a tube furnace for about 100 min at 800 °C by using $POCl_3$ as doping source. Then, the phosphosilicate glass was removed by HF solution (9% by volume). After that, SiN_x:H was deposited on the front surface as the antireflection and passivation layer by plasma enhanced chemical vapor deposition for 40 min at 400 °C. Finally, the fabrication of front and back electrodes were performed by the screen-printing, followed by a co-firing step at 750 °C for 30 s.

2.3. Characterization

The morphologies of the wafers were investigated by field emission scanning electron microscopy (FE-SEM) (Zeiss Ultra Plus). The reflectance spectra together with the internal quantum efficiency (IQE) and external quantum efficiency (EQE) were measured by QEX10 (PV MEASUREMENTS). And the electrical parameters of the solar cells were measured under AM1.5 spectrum at the temperature of 25 °C.

3. Result and discussion

3.1. The comparison of DWS and CMWS mc-Si wafers

Fig. 2(a–d) shows the SEM images of as-cut CMWS and DWS mc-Si wafers, together with the images of the wafers after a routine texture process. For as-cut CMWS wafers shown in Fig. 2(a), the surface damage features randomly distributed cracks and fissures. In contrast, irregular surface damage of parallel grooves, smooth areas, cracks and damaged pits is observed on as-cut DWS wafers [Fig. 2(b)]. Both as-cut CMWS and DWS wafers underwent the same HF/HNO_3 etching to remove the damage layer and form microstructures on the surface. As shown in Fig. 2(c), for as-etched CMWS wafers, wormlike pits with the size of about 3 μm in width are formed randomly on the whole surface. However, for as-etched DWS wafers, CM-T characterized by parallel grooves with different sizes closely formed on the Si surface is observed. Among them, the narrow grooves consist of elliptical pits with the opening size of about 2 μm in width while the elliptical pits oriented along the wide grooves are about 4 μm in width [Fig. 2(d)]. Although the saw marks are less noticeable compared with the as-cut ones, the HF/HNO_3 etching fail to eliminate them [see surface photos of as-cut DWS mc-Si wafers in Fig. 2(e) and HF/HNO_3 etched wafers in Fig. 2(f)].

3.2. Surface morphology by a new method based on MACE

In order to eliminate the saw marks and realize effective surface textures on DWS mc-Si wafers, systematic investigation was conducted in this work. Fig. 3 illustrates the SEM images of the

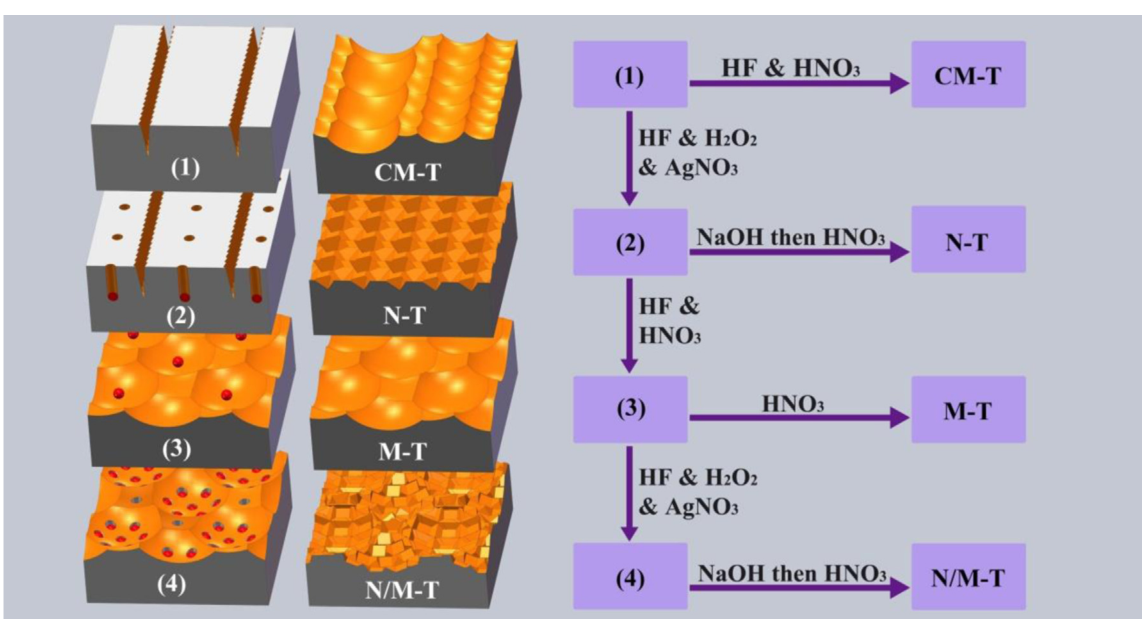

Fig. 1. Schematic illustration of the main steps preparing the CM-T, N-T, M-T and N/M-T on DWS mc-Si wafers.

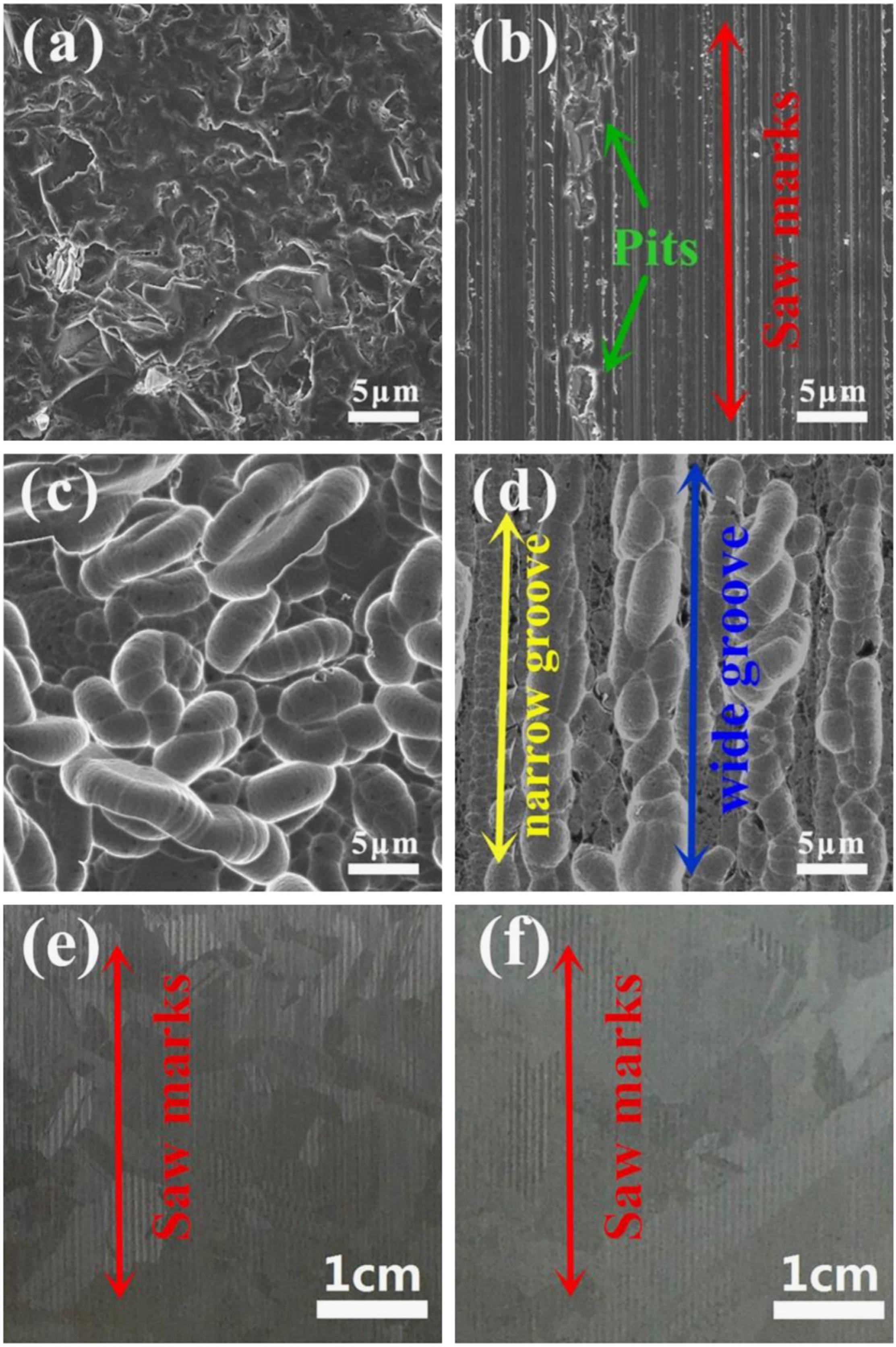

Fig. 2. SEM images of mc-Si wafers: (a) as-cut CMWS wafers (b) as-cut DWS wafers (c) routine textured CMWS wafers, and (d) routine textured DWS wafers. Surface photos of DWS mc-Si wafers: (e) as-cut wafers, and (f) HF/HNO_3 etched wafers.

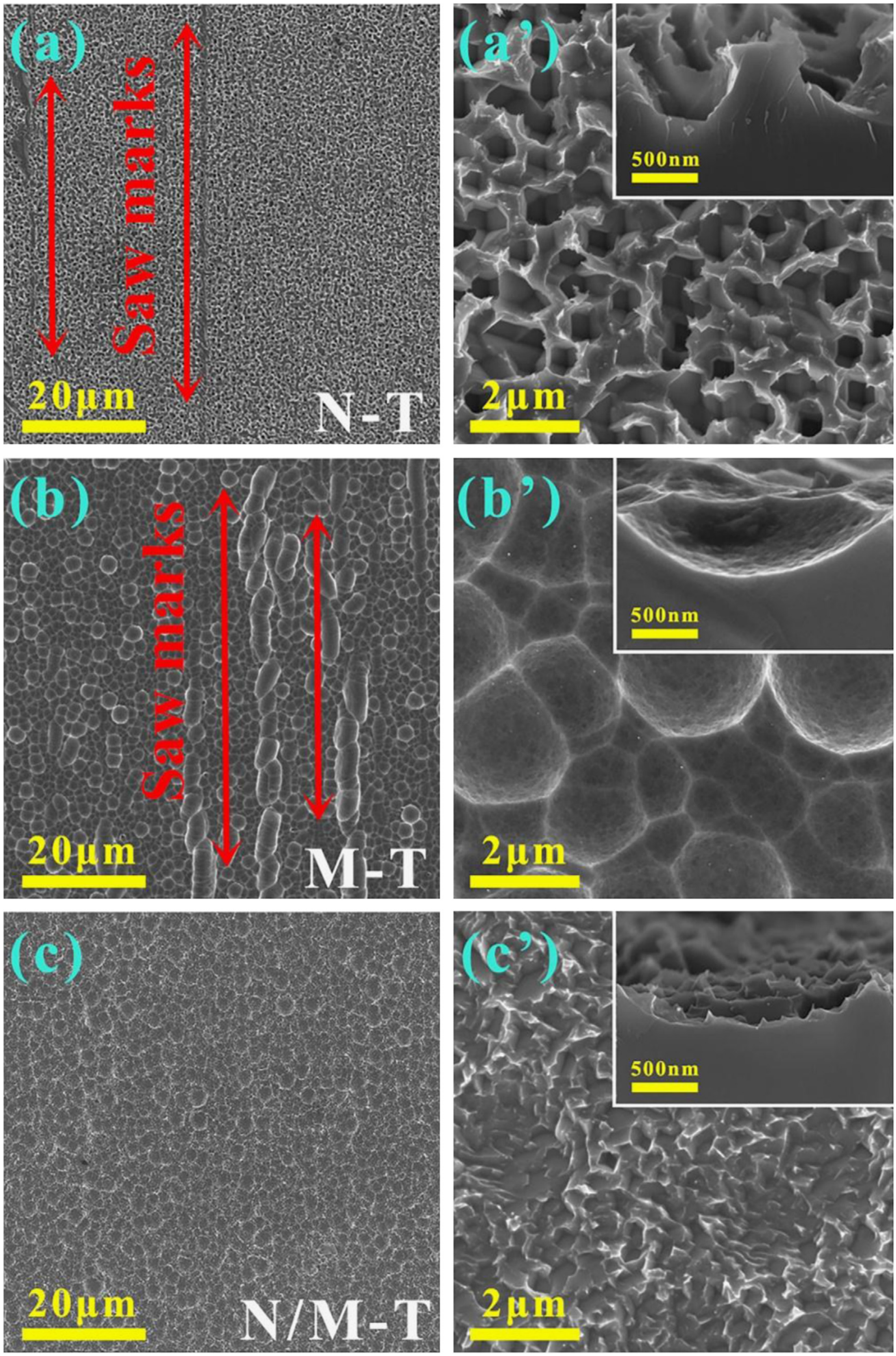

Fig. 3. SEM images of the textured wafers: (a) N-T, (b) M-T, (c) N/M-T. (a′)–(c′) are the enlargements of (a)–(c), together with the SEM images of the cross-section of the wafers in the inset.

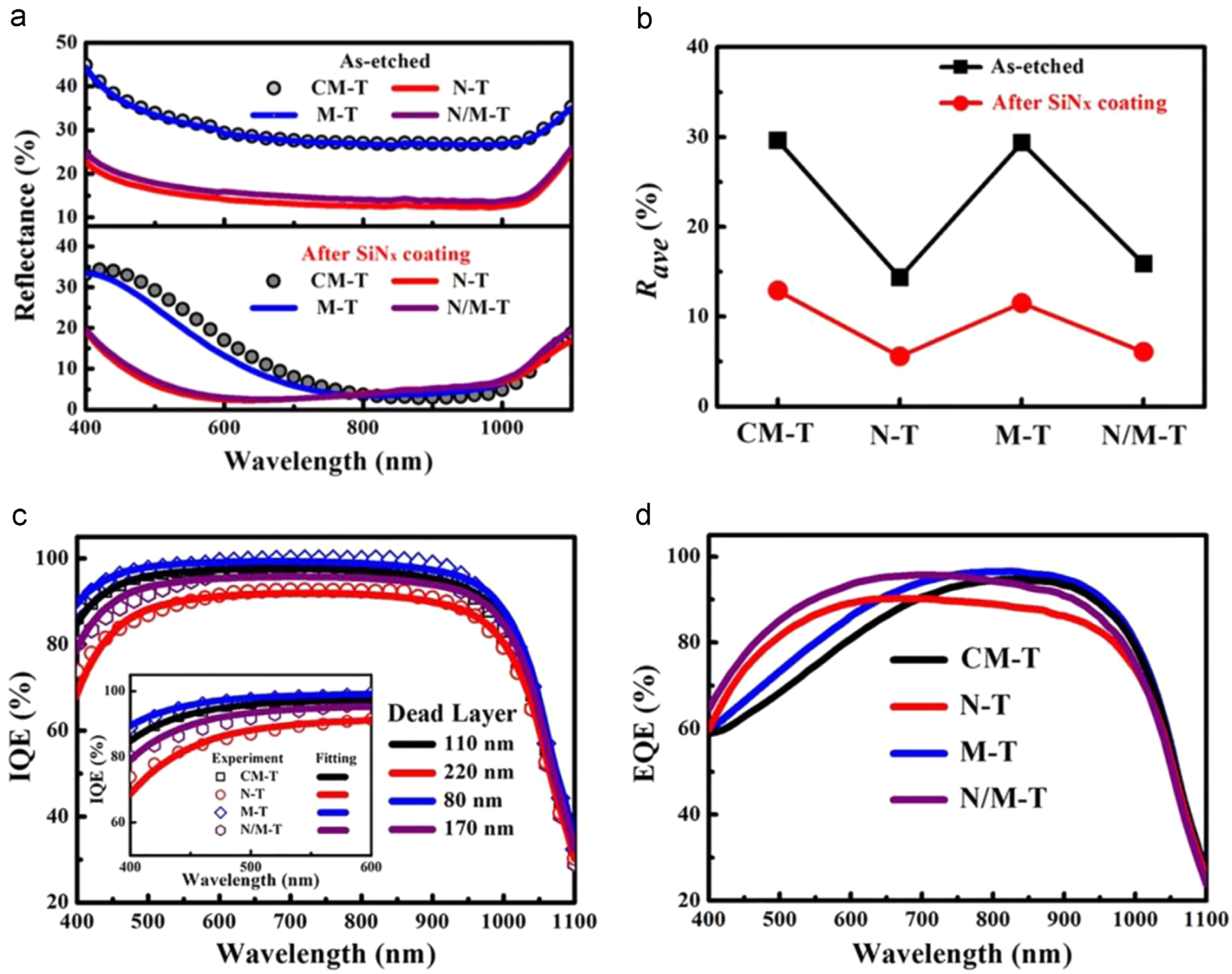

Fig. 4. (a) Reflectance spectra (400–1100 nm) of the as-etched and SiN_x-coated CM-T, N-T, M-T and N/M-T. (b) Averaged reflectance of the reflectance spectra shown in (a). (c) Experimental IQE and PC1D-fitting IQE of the CM-T, N-T, M-T and N/M-T based solar cells, together with the zoomed-in IQE spectra ranging from 400–600 nm in the inset. (d) Experimental EQE of the CM-T, N-T, M-T and N/M-T based solar cells.

textured DWS mc-Si wafers. By employing MACE technique, followed by NaOH etching, the saw marks are nearly removed [Fig. 3(a)] and inverted-pyramid-like N-T is formed [Fig. 3(a′)]. The average size of the N-T is about 700 nm in width and 600 nm in height. On the other hand, a group of the wafers are immersed in HF/HNO_3 solution after MACE process, leading to the formation of M-T as shown in Fig. 3(b) and (b′). The surface is covered with round pits with the size of about 2 μm in diameter and about 500 nm in height. Compared with CM-T, only few string structures can be found. In order to reduce the reflectance of the surface and enhance the optical gain, we have further fabricated N/M-T, which is characterized by nanostructures (about 400 nm in width) embedded in micro pits (about 2 μm in diameter), as illustrated in Fig. 3(c) and (c′). The structures are uniformly formed on the whole surface and no string structures can be found, which implies that all the saw marks are removed.

We propose the following chemical etching mechanism to understand how the saw marks are removed. MACE is a local electrochemical process with the metal particles acting as a local cathode and the Si substrate as the anode. In a typical MACE process, Ag nanoparticles are firstly deposited onto the surface of the Si substrate and inject holes into the valence band of Si, resulting in the oxidization of Si. Then the Si oxide is removed by HF. As a result, the Ag particles generate pits on the Si substrate. In the meantime, the surface is also etched by HF/H_2O_2. According to the results proved in Refs. [19–21], the dissolution rate of Si is faster at the Ag–Si interface than the one on Ag-free Si substrate due to the catalytic role of the Ag particles, leading to the expansion of pits under the Ag particles. With increasing etching time, the pits are expanded into cylindrical pores and the Ag particles sink at the bottom of the pores. On the one hand, after further etching in NaOH solution, inverted-pyramid-like N-T is formed owing to the anisotropic etching of Si. At the same time, general corrosion of the Si substrate helps to shallow the saw marks. On the other hand, HF/HNO_3 etching after MACE process is also effective in easing off the saw marks but forms sphere-like M-T. The cylindrical pores are enlarged and connected to each other, resulting in the elimination of the narrow saw marks, while deep saw marks become shallower due to the general corrosion of Si surface. After multiple-etching processes (sequentially, MACE process, HF/HNO_3 etching, MACE process and NaOH etching), all the saw marks are completely removed in N/M-T [Fig. 3(c)].

3.3. Optical characteristics and electrical analysis

As we all know, there are two main processes when the solar cell works, including generation of photocarriers and collection of photocarriers. In the former process, the optical character directly affects the number of the photons entering into the solar cells [15,22]. And electrical loss determines the number of the collected

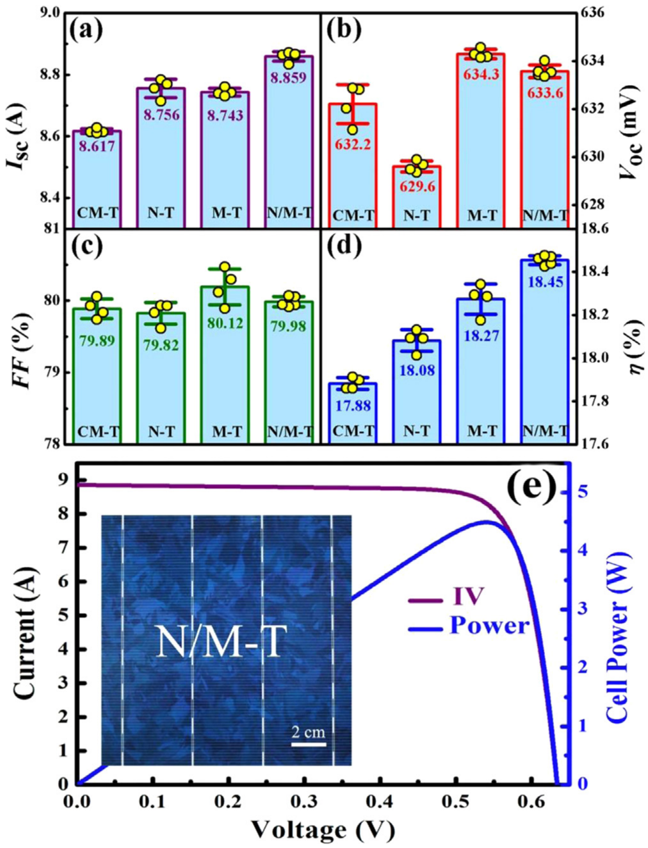

Fig. 5. Cell performance: (a) V_{OC}, (b) I_{SC}, (c) FF and (d) η for CM-T, N-T, M-T and N/M-T based solar cells. The yellow dots represent the experimental data while the height of the histograms represents the averaged value of the data. (e) I–V, P–V characteristics and the photograph of the highest-efficient N/M-T based DWS mc-Si solar cell. (For interpretation of the references to color in this figure legend, the reader is referred to the web version of this article.)

carriers in the latter process. Therefore, we investigate the influence of the surface structures on both optical and electrical properties to find an efficient texture for DWS mc-Si solar cells. Fig. 4(a) presents the reflectance spectra of the CM-T, N-T, M-T, and N/M-T for the as-etched and SiN_x-coated cases in the wavelength ranging from 400 nm to 1100 nm. For the as-etched cases, the reflectance of CM-T and M-T is nearly the same in the whole wavelength range while the reflectance spectrum of N-T is a little lower than the one of N/M-T. However, the reflectance of nanostructure contained surface (N-T and N/M-T) is much lower than the one of microstructure based surface (CM-T and M-T) in the whole wavelength range, which is attributed to the strong forward light scattering of the nanostructures in the short wavelength range and the gradual decrease of effective refractive index in the long wavelength range by the formed density-graded layer. For SiN_x-coated CM-T and M-T cases, antireflection effect is enhanced in the whole wavelength range, especially in the destructive interference region (about 750–950 nm). The reflectance is lower than 5% in this region but increases drastically in the short wavelength range with the highest value of about 35%. In contrast, for SiN_x-coated N-T and N/M-T cases, the reflectance at short wavelength is suppressed due to effective antireflection of the nanostructures and excellent broadband antireflection is achieved.

The averaged reflectance (R_{ave}) for the cases mentioned above is illustrated in Fig. 4(b). Here, R_{ave} is calculated by averaging the reflectance over the standard AM1.5 spectrum in the wavelength ranging from 400 nm to 1100 nm as follows:

$$R_{ave} = \frac{\int_{400\ \mathrm{nm}}^{1100\ \mathrm{nm}} R(\lambda)\cdot S(\lambda)\cdot \mathrm{d}\lambda}{\int_{400\ \mathrm{nm}}^{1100\ \mathrm{nm}} S(\lambda)\cdot \mathrm{d}\lambda} \quad (1)$$

where $R(\lambda)$ represents the experimental reflectance and $S(\lambda)$ represents the standard AM1.5 solar photon spectral distribution. The R_{ave} of the as-etched CM-T, N-T, M-T and N/M-T is 29.6%, 14.4%, 29.4% and 15.9%, respectively, and is reduced by a factor of 3 (11.4% for CM-T, 5.2% for N-T, 11.6% for M-T and 5.6% for N/M-T) after coating with SiN_x thin films. The results show that SiN_x coating is an effective technique to reduce reflectance on different structures.

On the other hand, in order to investigate the influence of morphology on electrical loss, the IQE of CM-T, N-T, M-T and N/M-T based solar cells is tested, as illustrated in Fig. 4(c), together with the corresponding ones simulated by PC1D. The inset presents the zoomed-in IQE spectra from 400–600 nm. It is found that the IQE decreases over the whole wavelength range with the formation of nanostructures, particularly at short wavelength. In addition, it is worth noting that the M-T based cells exhibit higher IQE, compared with CM-T based cells, suggesting that the elimination of the saw marks benefits the reduction of electrical loss. Actually, resulting from a "dead layer" (DL) from the heavily doped Si emitter [23], the surface and Auger recombination dominates the degradation of IQE in the short wavelength region. In our cases, we treat the nanostructures and the saw marks as a low lifetime DL and simulate the IQE with PC1D software to evaluate the DL thickness, as reported in the literatures [24,25]. Note that, our simulated IQE spectra match well with the experimental ones [see Fig. 4(c)], which guarantees the reliability. For N-T and N/M-T based cells, the thickness of the DL is 220 and 170 nm, respectively. The results indicate that the surface and Auger recombination becomes worse with the increasing height of nanostructures. Furthermore, M-T based cells exhibit a thinner DL of 80 nm, compared with that of CM-T based cells (110 nm), suggesting that eliminating the saw marks can reduce the electrical loss and enhance IQE.

Here, in order to evaluate the comprehensive influence of optical gain and electrical loss on cell performance, we illustrate in Fig. 4(d) the EQE data of the cells mentioned above. Obviously, the EQE of M-T is higher than that of CM-T in nearly the whole wavelength range, which implies that the elimination of the saw marks can significantly benefit the electrical performance of the cells. On the other hand, although suffering from worse surface recombination and Auger recombination, N-T and N/M-T based cells exhibit higher EQE at short wavelength attributed to remarkable antireflection effect of the nanostructures, compared with CM-T and M-T based cells. However, N-T based cells exhibit low EQE at long wavelength due to severe electrical loss. In contrast, for N/M-T based cells, the EQE value remains at a high level in the whole wavelength ranging from 550 nm to 950 nm, benefiting from the tradeoff between the optical gain and electrical loss.

3.4. Cell performance

Fig. 5(a–d) illustrates the measured output parameters including short circuit current (I_{sc}), open circuit voltage (V_{oc}), fill factor (FF) and η of the CM-T, N-T, M-T and N/M-T based DWS mc-Si solar cells (the yellow dots represent the experimental data while the height of the histograms represents the averaged value of the data.). Obviously, compared with CM-T based cells, all the N-T, M-T and N/M-T based cells exhibit higher I_{sc}, V_{oc} (except N-T based cells) and η, suggesting that our methods based on MACE are effective for the texturization of DWS mc-Si solar cells. For N-T based cells, the I_{sc} of 8.756 A is much higher than 8.617 A of CM-T based cells, which is attributed to the outstanding antireflection performance of the nanostructures, while the performance degradation of V_{OC} occurs due to the worse surface and Auger recombination. On the other hand, resulting from less electrical loss by eliminating the saw marks, M-T based cells exhibit high V_{OC} of 634.3 mV, which is higher by 2.1 mV compared with 632.2 mV of the CM-T based cells, together with I_{sc} of 8.743 A (higher than the one of CM-T based cells but a little lower than the one of N-T based cells). Moreover, benefiting from the tradeoff between optical gain and electrical loss, N/M-T based cells exhibit good performance in both I_{sc} and V_{oc} and thus possess the highest η of 18.45% among all the cells, which is higher by an absolute 0.57% compared with 17.88% of CM-T based cells. In addition, as shown in Fig. 5(c), the difference among the *FF* of the cells is not obvious, which implies that the surface morphology has nearly no influence on *FF*. Fig. 5(e) presents the current–voltage (*I*–*V*) and power–voltage (*P*–*V*) characteristics of the N/M-T based solar cell, together with the photograph of the cell. The maximum output power reaches 4.49 W on the wafer size of 243.36 cm^2, and the whole surface of the cell exhibits the color of dark blue, which is a satisfying color in industry.

4. Conclusions

In summary, DWS mc-Si wafers cannot be effectively textured by conventional methods due to the nonuniform etching of the saw marks, exhibiting high reflectance (about 12% in average after SiN_x coating) and poor electrical properties. In this work, we have presented effective texture methods for DWS mc-Si wafers based on MACE technique. We have successfully fabricated high-efficiency N-T, M-T, N/M-T based DWS mc-Si solar cells on the standard wafer size of 156×156 mm^2. From the study of optical characteristics, we find that the reflectance can be suppressed to a low level with the formation of nanostructures (about 5% in average after SiN_x coating), especially at short wavelength. However, at the same time, electrical loss from the surface recombination and Auger recombination becomes severe owing to the heavily doped Si emitter. Benefiting from the tradeoff between the optical gain and electrical loss, we have realized the N/M-T based DWS mc-Si solar cells with a high η of 18.45%, which is higher by an absolute 0.57% compared with 17.88% of CM-T based cells. Note that this technique also removes all the saw marks in DWS mc-Si wafers. Our work provides ways of fabricating DWS mc-Si solar cells with high efficiencies and satisfactory visual appearance.

Acknowledgments

This work was supported by the Natural Science Foundation of China (61234005, 11474201 and 11174202) and Natural Science Foundation of Jiangsu Province (BK20151284).

References

[1] W.H. Chen, X.M. Liu, M. Li, C.Q. Yin, L. Zhou, On the nature and removal of saw marks on diamond wire sawn multicrystalline silicon wafers, Mater. Sci. Semicond. Process. 27 (2014) 220.

[2] N. Watanabe, Y. Kondo, D. Ide, T. Matsuki, H. Takato, I. Sakata, Characterization of polycrystalline silicon wafers for solar cells sliced with novel fixed-abrasive wire, Prog. Photovolt. Res. Appl. 18 (2010) 485.

[3] B. Meinel, T. Koschwitz, J. Acker, Textural development of SiC and diamond wire sawed sc-silicon wafer, Energy Procedia 27 (2012) 330.

[4] W.I. Clark, A.J. Shih, C.W. Hardin, R.L. Lemaster, S.B. McSpadden, Fixed abrasive diamond wire machining—Part I: process monitoring and wire tension force, Int. J. Mach. Tools Manuf. 43 (2003) 523.

[5] A. Bidiville, K. Wasmer, R. Kraft, C. Ballif, Diamond wire-sawn silicon wafers-from the lab to the cell production, in: Proceedings of the 24th EU PV-SEC, 2009.

[6] X.G. Yu, P. Wang, X.Q. Li, D.R. Yang, Thin Czochralski silicon solar cells based on diamond wire sawing technology, Sol. Energy Mater. Sol. Cells 98 (2012) 337.

[7] K.X. Chen, Y.Y. Liu, X.S. Wang, L.J. Zhang, X.D. Su, Novel texturing process for diamond-wire-sawn single-crystalline silicon solar cell, Sol. Energy Mater. Sol. Cells 133 (2015) 148.

[8] A. Kumagai, Texturization using metal catalyst wet chemical etching for multicrystalline diamond wire sawn wafer, Sol. Energy Mater. Sol. Cells 133 (2015) 216.

[9] M. Lippold, F. Buchholz, C. Gondek, F. Honeit, E. Wefringhaus, E. Kroke, Texturing of SiC-slurry and diamond wire sawn silicon wafers by $HF–HNO_3–H_2SO_4$ mixtures, Sol. Energy Mater. Sol. Cells 127 (2014) 104.

[10] A. Stapf, C. Gondek, M. Lippold, E. Kroke, $HF–(NH_4)_2S_2O_8–HCl$ mixtures for HNO_3-and NO_x-free etching of diamond wire- and SiC-slurry-sawn silicon wafers: reactivity studies, surface chemistry, and unexpected pyramidal surface morphologies, ACS Appl. Mater. Interfaces 7 (2015) 16.

[11] F. Cao, K.X. Chen, J.J. Zhao, X.Y. Ye, J.J. Li, S. Zou, X.D. Su, Next-generation multi-crystalline silicon solar cells: diamond-wire sawing, nano-texture and high efficiency, Sol. Energy Mater. Sol. Cells 141 (2015) 132.

[12] S.A. Mann, M.J.D. Wild-Scholten, V.M. Fthenakis, The energy payback time of advanced crystalline silicon PV modules in 2020: a prospective study, Prog. Photovolt. Res. Appl. 22 (2014) 1180.

[13] K. Shirasawa, K. Fukui, K. Okada, Y. Inomata, H. Takahashi, Y. Fukawa, S. Fujii, Over 17% large area multicrystaline silicon solar cells, in: Proceedings of the 14th EU PV-SEC, 1997.

[14] D.S. Rubya, S.H. Zaidi, S. Narayanan, B.M. Damianid, A. Rohatgi, Rie-texturing of multicrystalline silicon solar cells, Sol. Energy Mater. Sol. Cells 74 (2002) 133.

[15] F. Toor, H.M. Branz, M.R. Page, K.M. Jones, H.C. Yuan, Multi-scale surface texture to improve blue response of nanoporous black silicon solar cells, Appl. Phys. Lett. 99 (2011) 103501.

[16] J.H. Oh, H.C. Yuan, H.M. Branz, An 18.2%-efficient black-silicon solar cell achieved through control of carrier recombination in nanostructures, Nat. Nanotechnol. 7 (2012) 743.

[17] Z.G. Huang, X.X. Lin, Y. Zeng, S.H. Zhong, X.M. Song, C. Liu, X. Yuan, W.Z. Shen, One-step-MACE nano/microstructures for high-efficient large-size multi-crystalline Si solar cells, Sol. Energy Mater. Sol. Cells 143 (2015) 302.

[18] S.H. Zhong, Z.G. Huang, X.X. Lin, Y. Zeng, Y.C. Ma, W.Z. Shen, High-efficiency nanostructured silicon solar cells on a large scale realized through the suppression of recombination channels, Adv. Mater. 27 (2015) 555.

[19] S.Y. Li, W.H. Ma, Y. Zhou, X.H. Chen, Y.Y. Xiao, M.Y. Ma, F. Wei, X. Yang, Fabrication of p-type porous silicon nanowire with oxidized silicon substrate through one-step MACE, J. Solid State Chem. 213 (2014) 242.

[20] Z.P. Huang, N. Geyer, P. Werner, J.D. Boor, U. Gösele, Metal-assisted chemical etching of silicon: a review, Adv. Mater. 23 (2011) 285.

[21] C. Chartier, S. Bastide, C. Le´vy-Cle´ment, Metal-assisted chemical etching of silicon in $HF–H_2O_2$, Electrochim. Acta 53 (2008) 5509.

[22] Z.G. Huang, S.H. Zhong, X. Hua, X.Y. Kong, N. Dai, W.Z. Shen, An effective way to simultaneous realization of excellent optical and electrical performance in large-scale Si nano/microstructures, Prog. Photovolt. Res. Appl. 23 (2015) 964.

[23] J.Y. Kim, M.K. Kwon, V.J. Logeeswaran, S. Grego, M.S. Islam, Post-growth in situ chlorine passivation for suppressing surface-dominant transport in silicon nanowire devices, IEEE Trans. Nanotechnol. 11 (2012) 782.

[24] X.X. Lin, X. Hua, Z.H. Huang, W.Z. Shen, Realization of high performance silicon nanowire based solar cells with large size, Nanotechnology 24 (2013) 235402.

[25] H.C. Yuan, V.E. Yost, M.R. Page, P. Stradins., D.L. Meier, H.M. Branz, Efficient black silicon solar cell with a density-graded nanoporous surface: optical properties, performance limitations, and design rules, Appl. Phys. Lett. 95 (2009) 123501.